



Photocatalytic activity of natural ground hematite in heterogeneous photo-Fenton process

Özkan Açıslı

Department of Petroleum and Natural Gas Engineering, Oltu Earth Sciences Faculty, Atatürk University, 25400 Oltu, Erzurum, Turkey, Tel. +90 442 816 4478-5940; Fax: +90 442 816 4479, email: ozkan.acisli@atauni.edu.tr

Received 4 February 2019; Accepted 29 June 2019

ABSTRACT

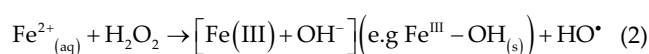
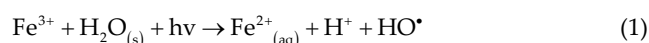
The removal of Malachite Green (MG) dye from aqueous solutions was examined in this study using natural ground hematite (Fe_2O_3) particles in heterogeneous photo-Fenton process. Within this scope, a natural hematite sample was first ground by a high-energy planetary ball mill. Photo-catalytic activity of the produced ultrafine particles was then studied with various processing variables such as catalyst dosage, initial dye concentration, H_2O_2 concentration, reusability and initial pH. Prior to the experiments, the prepared catalyst was characterized in many ways by means of numerous analytical techniques and measurement methods. Elemental and mineralogical analyses confirmed high hematite inclusion with a very low amount of quartz. The surface area increased to $65.547 \text{ m}^2 \text{ g}^{-1}$ as a result of the ball-milling process, pointing out improved catalytic property of the prepared sample. The experimental results indicated that the prepared catalyst provided a decolorization efficiency of 97.90% for the optimum conditions of 0.50 g L^{-1} catalyst dosage, 10 mg L^{-1} initial MG concentration, $15 \text{ mM H}_2\text{O}_2$ concentration and pH 11.0 at 120 min reaction time. Overall results suggested that, for the degradation of MG, natural ground hematite mineral can be effectively used as a heterogeneous catalyst in the photo-Fenton process due to the enhanced radiation scattering with respect to the classical process.

Keywords: Photo-Fenton; Hematite; Degradation of dye; Catalyst; Heterogeneous process

1. Introduction

The discharge of industrial organic dyes into the receiving body such as rivers and lakes leads to some irretrievable harmful effects in surface and ground waters [1]. Many different approaches including ion exchange, adsorption, precipitation and coagulation–flocculation have been tried so far, but none of these have provided promising results in terms of efficiency, economic feasibility and environmental concerns [2]. Advanced oxidation processes (AOPs) such as photo-catalytic [3,4], sono-catalytic [5,6] and Fenton [7,8] have attracted great attention from scientific community, and they are considered as a viable option for dye removal

due to their various advantageous properties. AOPs can effectively handle long-chain toxic compounds that are difficult to treat such as organic dyes. AOPs can degrade these compounds to various short-chain final products by means of HO^\bullet radicals generated [9–12]. In particular, heterogeneous photo-Fenton systems, one of the AOPs, are becoming increasingly important in this field [13,14]. In the presence of solid iron species and hydrogen peroxide under an irradiation source, reactive transient species, hydroxyl radicals, are generated in these processes. These radicals possess significant affinity for various kinds of refractory pollutants [15,16]. The main mechanism of the process can be expressed as follows [17–19]:



As indicated from the above equations, hydroxyl radicals can form by two ways in heterogeneous photo-Fenton process. In the first way, Fe³⁺ in the solution is reduced to Fe²⁺ under UV light, and hydroxyl radicals are formed which caused the degradation of dye. Secondly, Fe(II) reacts with H₂O₂ to form oxidized Fe(III) and additionally forms hydroxyl radicals depending on pH. In addition, Fe(III)–OH_(s) represents a hydroxylated solid form of the ferric iron, which would occur at the interface with water in Eq. (2) [13,17]. In the solution, Fe(III) may be dissolved, may form solid species or may precipitate on the surface of the existing oxide. In the solution, since oxidized and super-oxidized forms of iron are transient species, the hydroxyl radicals produced in the reaction are non-quantitative and it is dependent on pH [20–22]. Hematite as an iron-based solid catalyst that allowed the collection of UV light in the presence of peroxide was used in this study. The photo-Fenton processes do not require the use of excessive amounts of dissolved iron, and also allow the catalyst to be easily separated and recovered from treated wastewaters [23–26]. In the present study, the degradation of Malachite Green (MG) dye was investigated using natural ground hematite particles prepared by a high-energy ball mill in the heterogeneous photo-Fenton process under ultraviolet (UV-A) irradiation. The effects of catalyst dosage, initial dye concentration, peroxide concentration, reusability and pH on the decolorization efficiency were investigated in detail.

2. Experimental

2.1. Materials

The natural hematite sample was obtained from Karakaya Mineral Co., Turkey. MG dye was provided from Alvan Sabet Co., Iran. The main elemental composition of the natural hematite catalyst and the characteristics and chemical structure of MG are shown in Tables 1 and 2, respectively. Rest of the substances and reagents having analytical purity were provided from Merck Co., (Germany). Distilled water was used throughout the experiments.

2.2. Preparation of the Fe₂O₃ catalyst

The as-received hematite was first subjected to jaw and cone crushing. The crushed sample with top size of about 1 cm was then ground down to 100 μm by rod and

ball milling. The grinding product was further ground for 2 h at 900 rpm using a high energy planetary ball mill (LB 200, Turkey). The final product, having an average size of 1,000 nm, was stored in closed containers until its use in the experiments.

2.3. Characterization of the catalyst

The prepared catalyst was characterized in detail using various analyses and measurements. X-ray diffraction (XRD) patterns were recorded using a PANalytical Empyrean instrument (USA) with Cu-Kα radiation (40 kV, 30 mA, 1.54051 Å) over 10°–70° at room temperature. The scanning rate of the instrument was kept constant as 2°min⁻¹. Fourier transform infrared spectroscopy (FT-IR) analysis was carried out with a Tensor 27, Bruker instrument (Germany) using the KBr pellet technique in 4,000–400 cm⁻¹. Scanning electron microscopy (SEM) images and elemental inclusions of the natural hematite catalyst were examined by a Zeiss Sigma 300 instrument associated with energy dispersive X-ray (EDX) spectroscopy (Germany). In addition to these analyses, specific surface area measurement was done by a Micromeritics 3 Flex instrument (USA) using nitrogen adsorption–desorption isotherms at –197.2°C with the relative pressure varying from 0 to 1. The measurement was evaluated based on the Brunauer–Emmett–Teller (BET) and Barrett–Joyner–Halenda (BJH) methods. Particle size and its distribution were measured using a Zeta-sizer Nano ZSP.

2.4. Experimental setup and the procedure

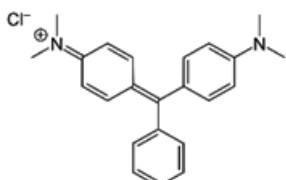
Photo-Fenton experiments were conducted in a magnetically stirred quartz cylindrical reactor with the working volume of 500 mL. Magnetic stirring was used to achieve effective interaction between the catalyst and the dye. Outer surface of the reactor was completely covered with aluminum foil to obtain the maximum efficiency from the UV source. The experimental setup used is illustrated in Fig. 1. 16 W UV-A (Sylvania, Japan) was used as the UV irradiation source. Batch studies were carried out with the constant MG solution of 500 mL to determine the effects of various processing variables, catalyst dosage (0.20–0.60 g L⁻¹), peroxide concentration (0–25 mM), initial MG concentration (10–50 mg L⁻¹) and pH (3–11), on the decolorization efficiency of MG. The pH value was adjusted by adding 0.1 M H₂SO₄ or NaOH solution using a pH meter.

Experimental procedure started with the addition of certain amount of the prepared catalyst and H₂O₂ in the predetermined concentration of MG solution that was formerly poured into the reactor.

Table 1
Main elemental composition, zeta potential and conductivity of the sample

Element	O	Mg	Ca	Si	Mn	Fe
Weight (%)	31.49	1.19	2.57	3.36	0.83	60.57
T°C	ZP mV	Mob μm cm Vs ⁻¹	Cond mS cm ⁻¹	Quality factor		
25	-9.25	-0.725	0.0191	2.71		

Table 2
Chemical structure and basic characteristics of MG

C.I. name	Chemical formula	Chemical structure	MW (g mol ⁻¹)	λ_{\max} (nm)
Malachite Green	C ₂₃ H ₂₅ ClN ₂		364.917	618

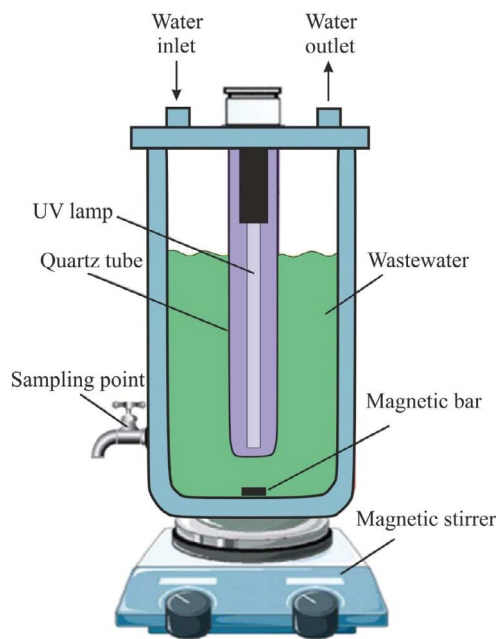


Fig. 1. Experimental setup used for photo-Fenton process.

The suspension was then agitated in dark for 20 min to reach the equilibrium. Afterward, the UV-A lamp was placed into the reactor and turned on. In addition, the tests conducted without UV irradiation were also performed in covered beakers to ensure similar processing conditions with the photo-Fenton experiments. At the predetermined time intervals, approximately 3 mL solution was taken and then centrifuged at 5,000 rpm for 4 min. In order to stop the Fenton reactions in the filtrate, 0.5 mL methanol was added into the solution. The remaining MG concentration was finally measured using an Optizen Pop UV-Vis spectrophotometer. The removal efficiency (RE, %) of MG was calculated from the below equation:

$$RE(\%) = \left[\frac{C_0 - C_t}{C_0} \right] \times 100 \quad (3)$$

where C_0 is the initial dye concentration and C_t is the MG concentration at time t .

Adsorption experiments were performed using temperature-controlled thermostatic shaker (VWR, Belgium) without UV radiation. Point of zero charge (pH_{pzc}) of the natural

hematite particles was determined based on the method suggested by Bessekhouad et al. [27] with some minor modifications. According to this method, a total of 10 separate NaCl solutions (0.01 M 50 mL) were first prepared, and the pH values were adjusted from 3 to 11 with HCl and NaOH solutions. 0.2 g hematite was then added to each solution which was then stirred at 150 rpm for 48 h in a thermostatic shaker (VWR, Belgium). At the end of the residence time, the final pH values of each solution were measured, and the difference between the initial and final pH values (ΔpH) was plotted against initial pH values. The point at which ΔpH was equal to zero is the pH_{pzc} .

3. Results and discussion

3.1. Characterization of natural Fe₂O₃ catalyst

Fig. 2 shows XRD patterns of the hematite sample. According to the XRD analysis, the crystallinity and the peaks correspond to the rhombohedral phase of hematite [28]. The peaks at 2θ values of 24.2°, 33.1°, 35.7°, 40.8°, 49.5°, 54.0°, 57.5°, 62.7° and 64.1° were indexed as the respective diffractions of 012, 104, 110, 113, 024, 116, 018, 214 and 030, which were attributed to standard diffraction spectrum of hematite (These index hkl based on ICSD no. 201096) [29].

FT-IR spectra of the hematite sample are shown in Fig. 3. As seen from this figure, the IR absorption bands can be characterized by the sharp peaks of 430 and 530 cm⁻¹, which are resulted from the Fe–O stretching vibrations [30,31]. The peak at about 1,040 cm⁻¹ is resulted from silica stretching modes as Si–OH and Si–O–Si groups [31]. The first broad peak at about 3,200 cm⁻¹ is assigned to OH stretching mode group. These peaks, which reflect the water content in a structure, are due to iron hydroxides of the sample [31,32]. The sharp peak observed between 1,600 and 1,300 cm⁻¹ can be attributed to the C=O asymmetric and symmetric bending vibration of carbonyl groups [33].

3.2. Morphological and particle size distribution analyses

SEM images of the prepared natural hematite particles are shown in Fig. 4. As seen from the SEM micrographs, particles are predominantly agglomerated and have partially rough surfaces. As can be seen from the results of the BET analysis in Table 3, the porosity is caused by the formation of inter-particle spaces [19]. The SEM images also indicate that the particles are not uniform in both shape and size. As displayed in the nanoscale SEM images and in the particle size distribution analysis (Fig. 5), the prepared catalyst is

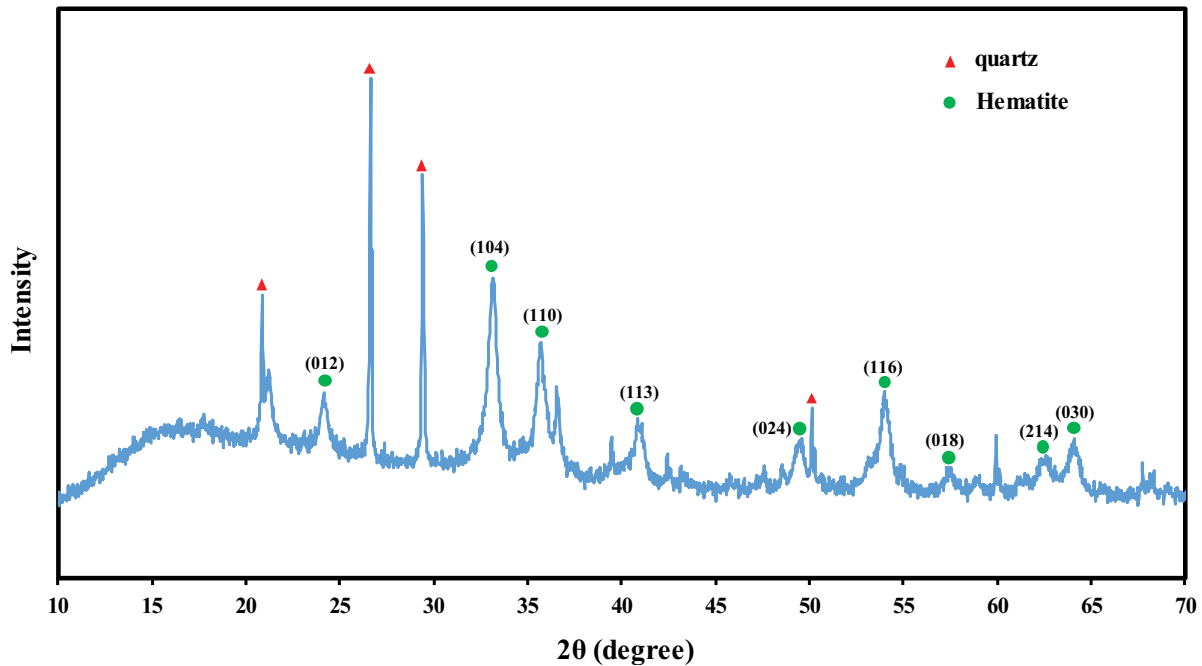


Fig. 2. XRD patterns of the natural hematite sample.

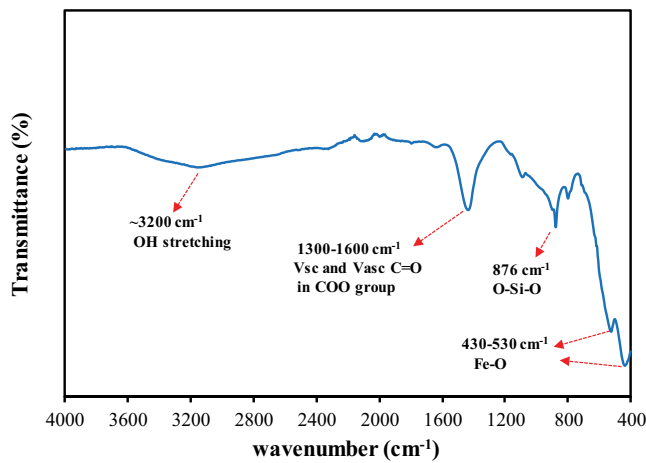


Fig. 3. FT-IR spectra of the natural hematite ore.

generally composed of particles with sizes of approximately 1,000 nm. These results are also supported by the results of particle size distribution, which are reported in Table 3. EDX spectra of the sample can be seen from Fig. 6. According to the EDX analysis, the particles contain mainly Fe and O elements. Since the cumulative weight percentages of these two elements are more than 92%, the sample used can be considered as quite pure.

3.3. Surface area and pore size analysis

In this stage, total pore volume of the sample was measured for the single point P/P_0 value of 0.950, and the pore size distribution was determined by the Barrett–Joyner–Halenda (BJH) method. The hematite samples were degassed

for 15 h at 100°C before the measurements. As seen from Table 3, the obtained results indicated that hematite sample is mesoporous, which may be the reason for its high catalytic activity [34].

Fig. 7 shows the N_2 adsorption/desorption BET isotherm of the prepared catalyst. Based on the IUPAC classification, the isotherm results exhibit a type-IV isotherm and H3 hysteresis loop for the P/P_0 value of 1.0. The Type H3 loop has mainly two characteristic features:

- It has an adsorption branch, which resembles type II isotherm.
- It has the lower limit of desorption branch, which is located in the P/P_0 caused by cavitation-induced.

This type of loops is resulted from either non-rigid aggregates of flat-shaped particles or macro pores which partially contribute pore density [35]. These results point out that the catalyst has the macro porosity-scale pores. Fig. 8 exhibits the pore size distribution of the prepared sample, indicating that the pore volume was mainly distributed in the particles finer than 10 nm.

3.4. Effect of operational parameters on the photo-Fenton process

3.4.1. Catalyst dosage

The amount of catalyst has generally significant effect on photo-Fenton processes. For this reason, hematite dosages varying from 0.20 to 0.60 g L⁻¹ were tested to determine its optimum. Fig. 9 illustrates the effect of hematite catalyst dosages on the decolorization efficiency of MG. According to Fig. 9b, for the residence time of 120 min, with increasing natural hematite particle dosage from 0.20 to 0.60 g L⁻¹, the decolorization efficiency increased from 81.40% to 96.34%,

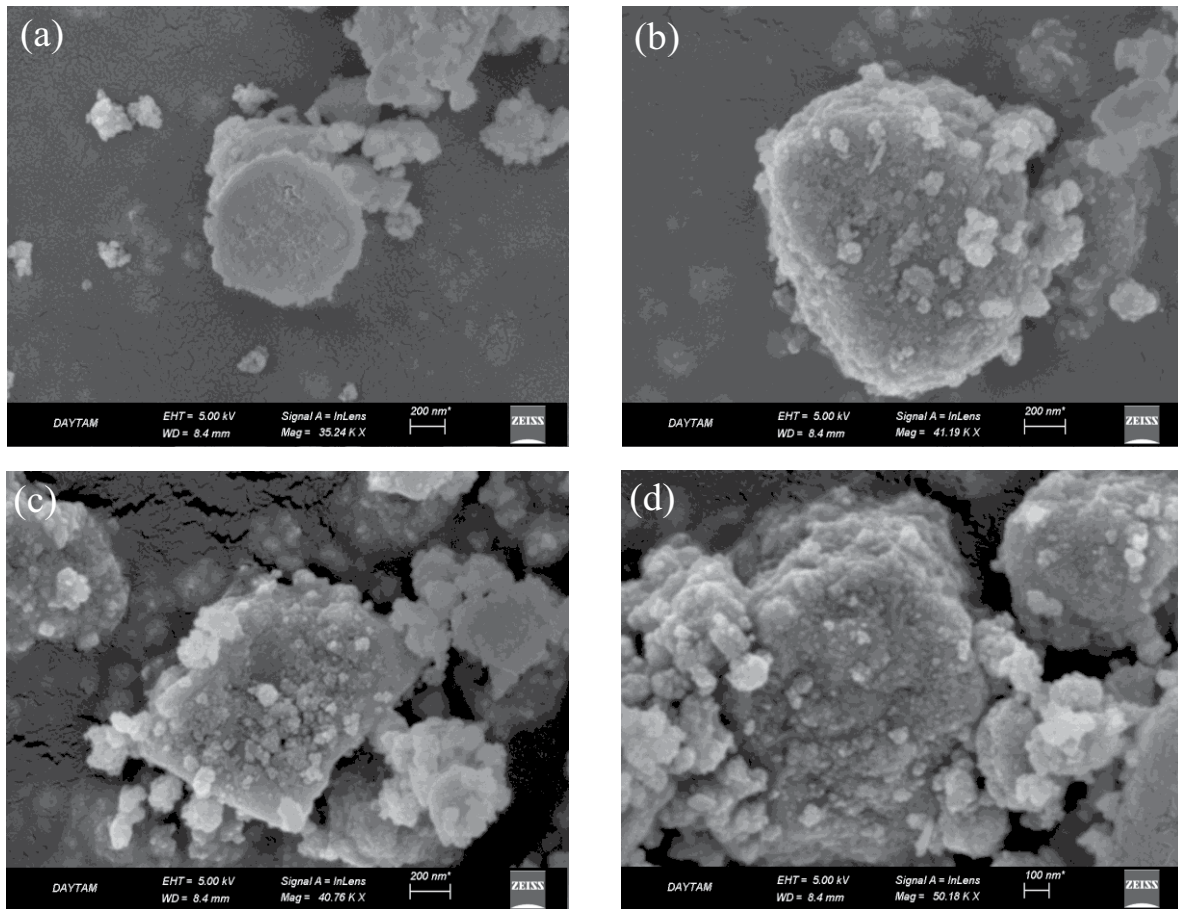


Fig. 4. SEM micrographs of the natural hematite particles.

Table 3
Results of the surface area measurements

Parameter	Values
BET surface area ($\text{m}^2 \text{g}^{-1}$)	65.547
BJH cumulative surface area ($\text{m}^2 \text{g}^{-1}$)	40.094
Total pore volume ($\text{cm}^3 \text{g}^{-1}$)	0.070
Average pore width (nm)	4.261

respectively. As the dosage of the natural hematite catalyst increases, the formation of hydroxyl free radical required for catalytic degradation of the target organic pollutant increases due to the increased number of active reaction sites [36,37].

However, although the amount of catalyst increased from 0.50 to 0.60 g L^{-1} , there was no significant increase in the decolorization efficiency of the dye. This is due to the fact that when the amount of natural hematite particles exceeds a certain level of saturation stage, the light effect of the photon decreases radially. This situation probably creates a light scanning effect that leads to a reduction in the surface area exposed to excessive photocatalyst irradiation [38,39]. In such processes, the increase in the amount of catalyst can sometimes reduce the decolorization efficiency

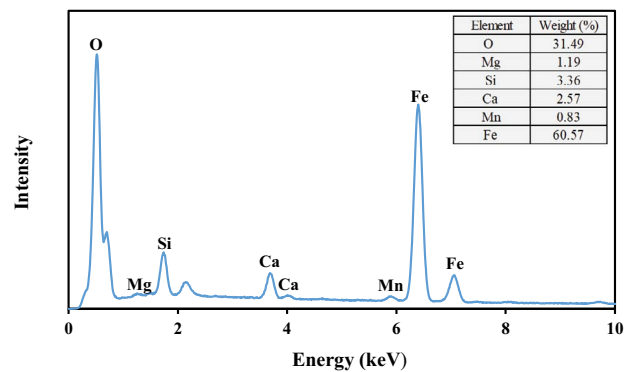


Fig. 5. EDX spectra of natural hematite particle samples.

or cause an insignificant increase. This is due to the reduced amount of free radical due to the scavenging potential of iron ions [36]. In addition, an excess amount of catalyst can lead to increased turbidity of the solution, which reduces the reaction of photo-Fenton [40].

3.4.2. Initial dye concentration

Degradation performance largely depends on chemical structure and concentration of target compound, and other

existing substances in solution [39]. Some compounds such as 4-chlorophenol need a longer reaction time due to the complexity of its intermediate products with respect to oxalic acid, which is directly mineralized to carbon dioxide

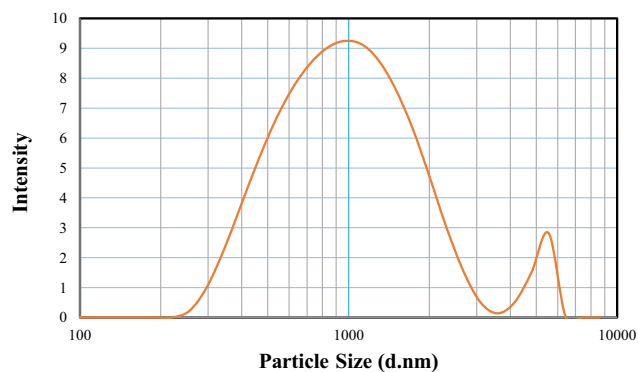


Fig. 6. Particle size distribution of the ground sample.

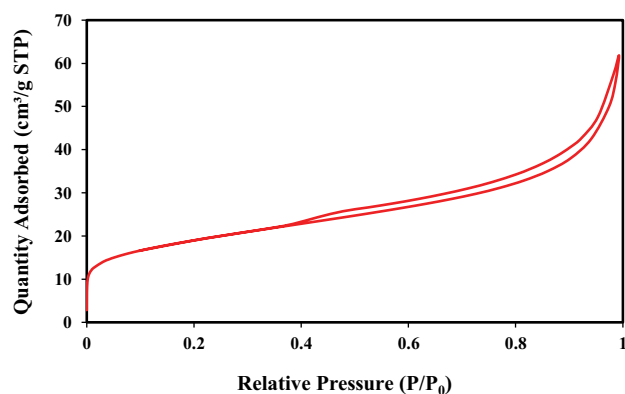


Fig. 7. Isotherms of N₂ adsorption/desorption of natural hematite samples.

and water [41]. Fig. 10 shows variability of the decolorization efficiency with MG concentrations ranging from 10 to 50 mg L⁻¹. As revealed in Fig. 10b, when the dye concentration decreased from 50 to 10 mg L⁻¹, the decolorization efficiency increased from 53.29% up to 94.62% for 120 min, respectively. This is most probably resulted from the insufficient hydroxyl free radicals to decompose high MG concentrations under the constant values of the operational parameters. The increased dye concentration can also saturate the particle surface of the natural hematite catalyst, and therefore it can lead to a reduction in the photonic efficiency and result in deactivation [42]. In addition, if the more effective the pollutant adheres to the catalyst surface, the easier its removal from the solution. Hence, functional groups of pollutants are highly important in photo-catalytic degradation [43].

3.4.3. Kinetics of the degradation process

In this stage, the kinetic studies were conducted using the Langmuir–Hinshelwood (LH) model, which is one of the

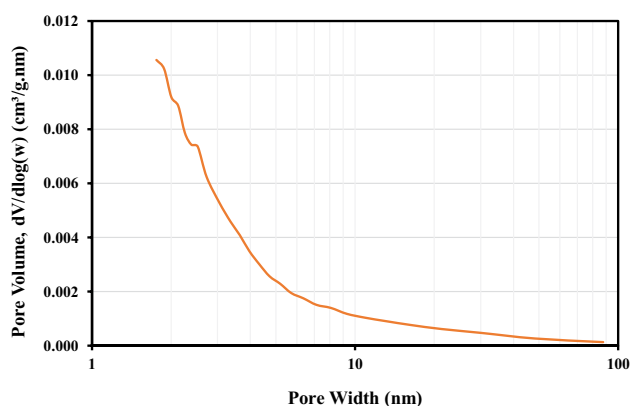


Fig. 8. BJH pore size distribution of the natural hematite samples.

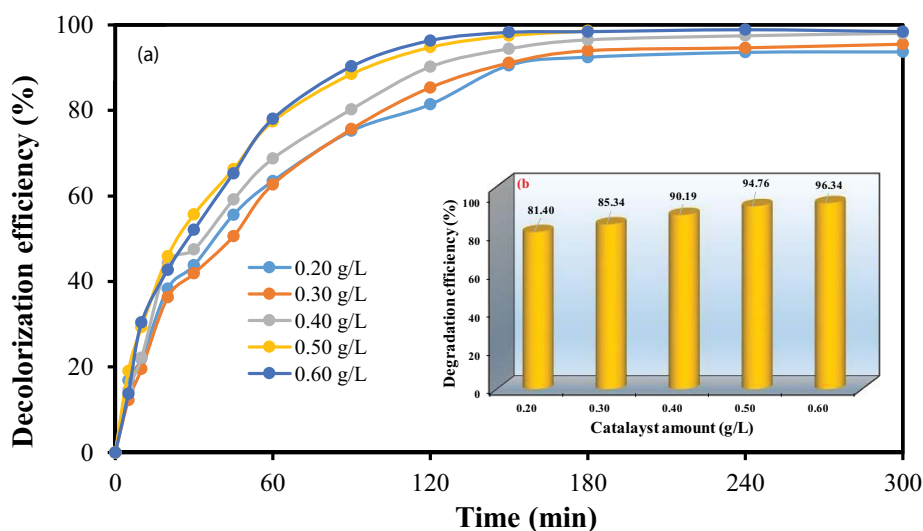


Fig. 9. Effect of catalyst amount of degradation efficiency of MG under the photo-Fenton process (a) as a function of time and (b) for 120 min. Experimental conditions: [MG]₀: 10 mg L⁻¹, temperature: 20°C, natural pH: 9.30, [H₂O₂]: 15 mM (1.5 mL L⁻¹, 30%).

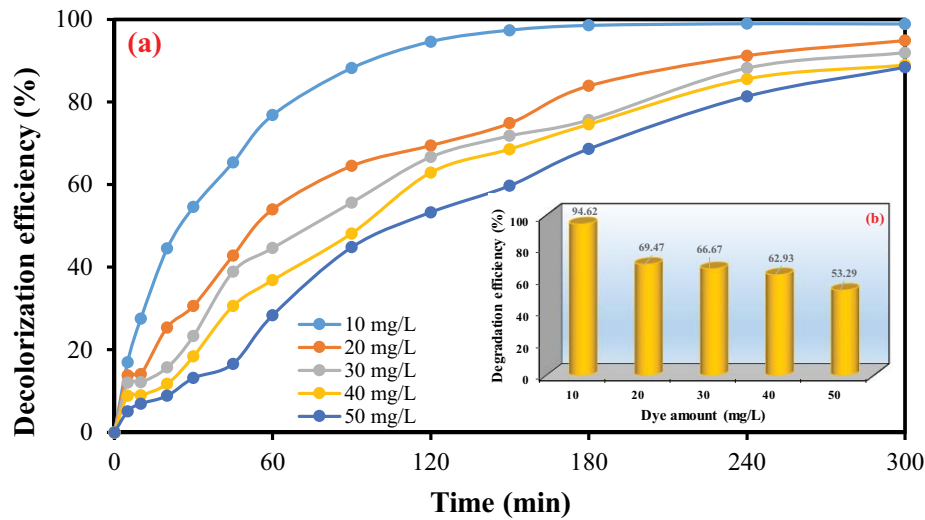


Fig. 10. Effect of initial dye concentration on the degradation efficiency (a) as a function of time and (b) for 120 min. Experimental conditions: catalyst dosage = 0.50 g L⁻¹, [H₂O₂]₀ = 15 mM and natural pH: 9.30, temperature: 20°C.

most commonly used approaches for the characterization of heterogeneous catalytic processes [17]. The equations used to build this model are as follows [44]:

$$r = -\frac{dC}{dt} = \frac{k_r KC}{1 + KC} \quad (4)$$

$$\ln\left(\frac{C_0}{C}\right) = k_r K t = k_{app} t \quad (5)$$

$$\frac{1}{k_{app}} = \frac{1}{k_r K} + \frac{C}{k_r} \quad (6)$$

where k_r is the reaction rate constant (mg L⁻¹ min⁻¹), t refers to the irradiation time (min), C_0 and C indicate the respective

dye concentrations at initial and a specific time (mg L⁻¹), K represents the equilibrium constant (L mg⁻¹) and k_{app} is the pseudo-first-order rate constant (min⁻¹).

When $\ln(C_0/C)$ is plotted against time, it gives a straight line with the high correlation efficiency ($R^2 > 0.99$) illustrated in Fig. 11, which confirms the suitability of the model for the obtained test results [45]. The reaction rate constants (k_{app}) decreased with the increasing dye concentrations. In particular, the rate constants of 0.0193, 0.0101, 0.0086, 0.0077 and 0.0068 min⁻¹ were obtained for the sequential MG concentrations of 10, 20, 30, 40 and 50 mg L⁻¹. In addition, when initial concentration was plotted against $1/k_{app}$, the reaction rate constant (k_r) and the adsorption equilibrium constant (K) were found as 0.45177 mg L⁻¹ min⁻¹ and 0.0522 L mg⁻¹, respectively. The high regression coefficient (0.9232) obtained also supports the suitability of the Langmuir–Hinshelwood kinetic model.

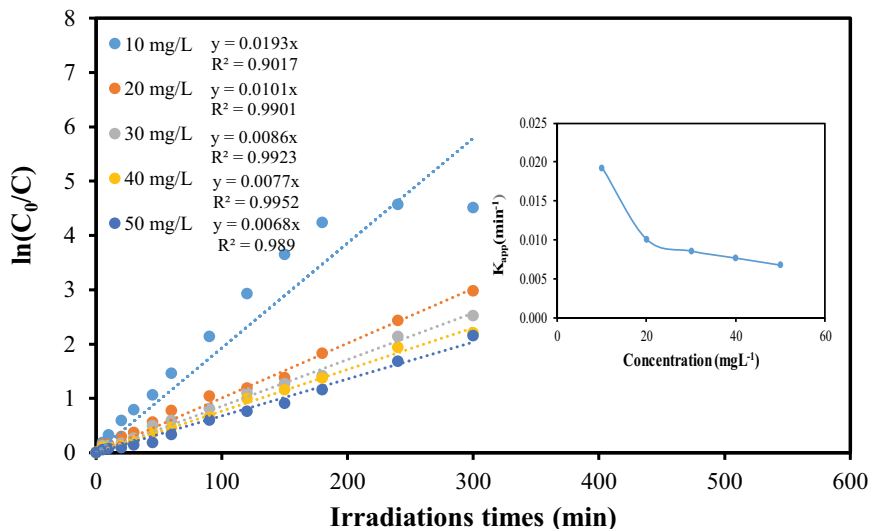
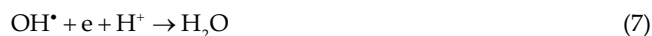


Fig. 11. Kinetics of Malachite Green degradation for different initial concentrations in the presence of hematite catalyst. Inset shows the relationship between the apparent rate constants and initial concentrations of MG.

3.4.4. Effect of initial pH

The initial pH is an important parameter since it influences precipitation of the iron oxides present in the catalyst and changes the surface properties of the catalyst. In addition, pH determines the ligands of dissolved iron complexes which affect the light absorbance property [40]. The experiments were carried out with 0.50 g L⁻¹ catalyst dosage, 15 mM H₂O₂ concentration and 50 ppm initial MG concentration. As clearly seen from Fig. 12, the decolorization efficiencies of 23.64%, 81.37%, 84.47%, 88.74%, 81.66% and 97.90% were obtained for the respective pH values of 3, 4, 5, 7, 9 and 11 for the elapsed time of 120 min. The decolorization efficiency depends on the pH of the media in the photo-Fenton-like processes. As seen in Fig. 13, the zero point charge (pH_{pzc}) of the natural hematite was found to be around 8.0–9.0. This is meaning that the catalyst surface is positively charged below the pH of 8.0–9.0 whereas it is negative above the pH_{pzc}.

As seen in Fig. 13, for pH values lower than 8.0, the hematite catalyst surface charge is positively charged, causing a reduction in the adsorption efficiency due to the electrostatic repulsion [46]. As shown in Fig. 13, the low decolorization efficiency of MG at pH value of 3.0 may be attributed to the scavenging effect of hydrogen ions at strongly acidic conditions as shown in Eq. (7) [47] as follows:



In contrast, a significant increase in the adsorption of cationic MG was observed due to the negative surface of the catalyst at high pH. For example, the increase in decolorization efficiency at pH of 11 can be attributed to the enhancement in adsorption of cationic MG dye molecules by the combination of electrostatic interactions and hydrogen bonding through strongest interaction.

Similar results have also been reported by Öztürk and Malkoc [48]. Moreover, the increment of adsorption capacity at pH higher than 9.0 would probably be due to the alkaline fading of MG for that MG turns into a carbinol base at a basic pH [49].

As a result, at high pH, due to the reduction of Fe⁽³⁺⁾ ion concentration and increased Fe(OH)₃ in the solution, the decolorization efficiency of MG is expected to decrease; whereas the opposite situation can be attributed to both the effective adsorption process and color fading. The decolorization efficiency of cationic MG dye demonstrates that it strongly depends on pH of the solution and the point of zero charges (pH_{pzc}) of the catalyst.

3.4.5. Effect of H₂O₂ concentration

Since hydrogen peroxide is particularly important in the generation of hydroxyl radicals, it was evaluated as

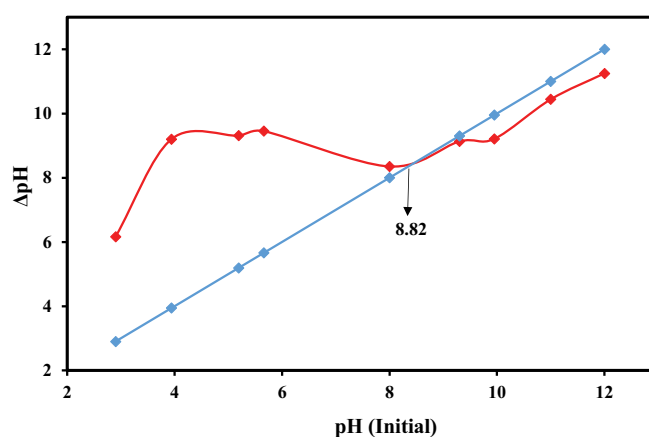


Fig. 13. pH_{pzc} plot of the natural hematite sample.

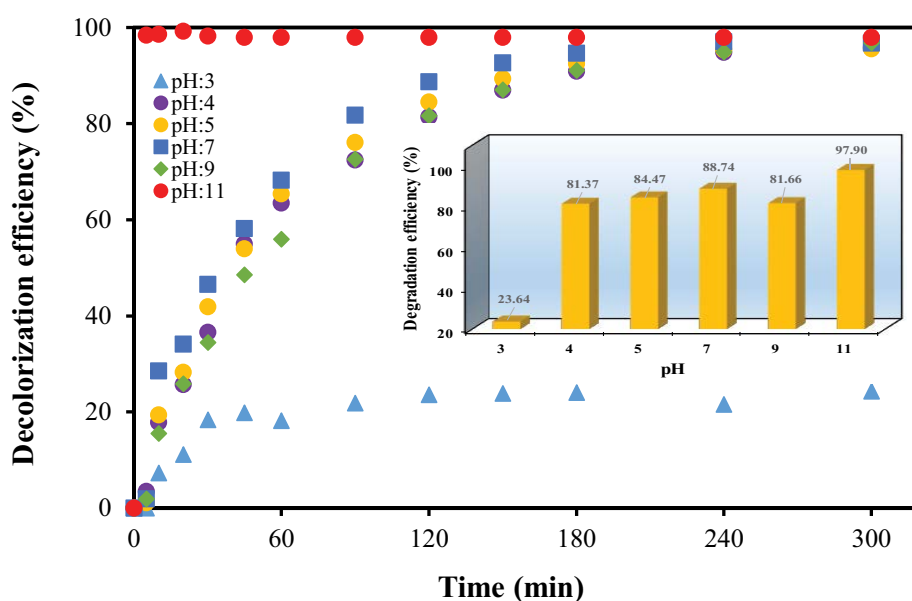


Fig. 12. Effect of initial pH on the degradation efficiency of MG. Experimental conditions: catalyst dosage = 0.50 g L⁻¹, [H₂O₂]₀ = 15 mM and [MG]₀ = 50 ppm.

an indispensable parameter for Fenton processes. For this reason, the effect of peroxide concentration (0–25 mM) was tested as a function varying processing time up to 120 min for the hematite catalyst dosage of 0.50 g L⁻¹, initial MG concentration of 10 mg L⁻¹ and natural pH of 9.30 to determine its optimum value.

As seen from Fig. 14b, the decolorization efficiency values of 45.38%, 74.57%, 83.47%, 94.62%, 85.90% and 90.46% were obtained for the respective peroxide concentrations of 0, 5, 10, 15, 20 and 25 mM at reaction time of 120 min. Based on these results, peroxide concentration of 15 mM was selected as the optimal value for performing photo-Fenton process over natural hematite catalyst. As can be clearly seen from Fig. 14b, H₂O₂ addition from 0 to 15 mM resulted in the increase of MG decolorization efficiency from 45.38% to 94.62% within 120 min. Possible explanation for this improvement is the generation of higher amounts of radicals by decomposition of H₂O₂ in magnetite presence [33,50]. Hydrogen peroxide molecules in the media act as a source for the generation of hydroxyl radicals by the dissociation of water molecules; thus, the increase in the concentration of H₂O₂ increases the production of hydroxyl radicals [36]. However, an increase higher than optimum value can slow the degradation process. The main reason is that the excessive amount of H₂O₂ can act as scavenging compound for hydroxyl free radicals by producing H₂O₂ that is less active than the hydroxyl radical [36,51]. Thus, excessive amounts of H₂O₂ in the solution react with OH[•] resulting in the generation of weak OOH[•] radicals as represented in Eqs. (8) and (9) [36,45].



So, in the present study, 15 mM of hydrogen peroxide can efficiently assist the photo-Fenton process to degrade 10 mg L⁻¹ of MG in the presence of 0.50 g L⁻¹ of the natural hematite catalyst.

3.4.6. Single effect of each component

The efficiencies of various processes involved in the removal of MG through the photo-Fenton process catalyzed by natural hematite were compared, and the obtained results are given in Fig. 15. As shown, the degradation of MG solution was insignificant in the dark within an elapsed time of 120 min. Generally, photonic process alone is not efficient enough to degrade organic compounds in the solution. As shown in Fig. 15, the decolorization efficiency of MG for 50 mg L⁻¹ solution was determined as 0.77% in the presence of only UV irradiation at 120 min. This effect increased by 3.75% with the addition of peroxide. From the data obtained, it was observed that the adsorption of Mg was quite high on the natural hematite catalyst. This value was determined as 54.78% for 300 min and 18.81% for 120 min. When the peroxide is added to the solution containing the catalyst, the decolorization efficiency of Mg significantly increased and when the time increased from 120 to 300 min, the decolorization rate reached from 53.29% to 88.40%.

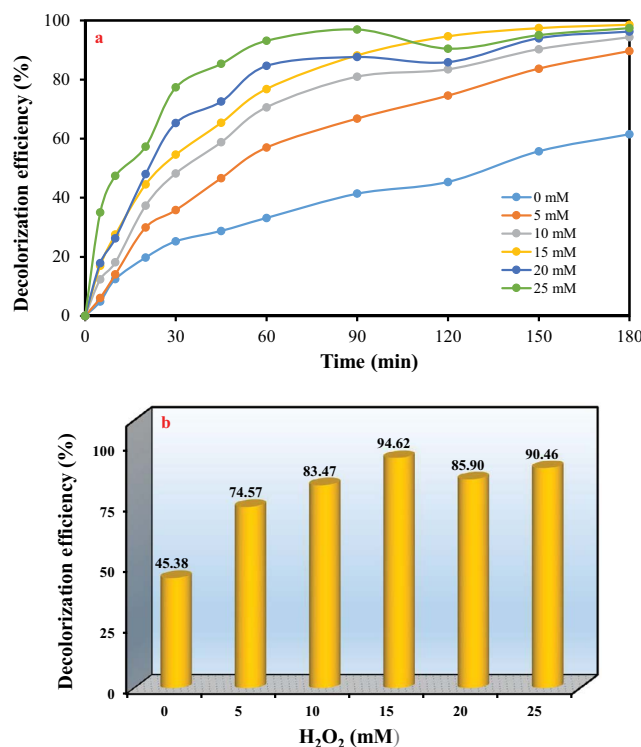
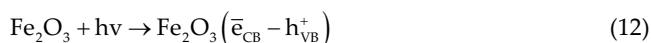


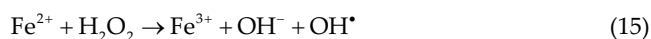
Fig. 14. Effect of H₂O₂ concentration on the degradation efficiency of MG (a) as a function of time and (b) for 120 min. Experimental conditions: catalyst dosage = 0.50 g L⁻¹, [MG]₀ = 10 mg L⁻¹ and natural pH: 9.30, temperature: 20°C.

However, the photo-Fenton process, formed by means of inserting UV-light to the process, provided a great MG deterioration in a very short time. Naturally, the photo-Fenton reactions were originated from the light absorptions by hematite or dye.

The excited hematite or dye produced electron in conduction band, which was then absorbed by H₂O₂ to produce HO[•] radical [52,53]. Alternatively, the photo-generated electron was trapped by Fe³⁺ to form Fe²⁺, which reacted with H₂O₂ (similar to Fenton reaction) to produce HO[•] radicals based on Eqs. (10)–(16) [54–56].



Or,



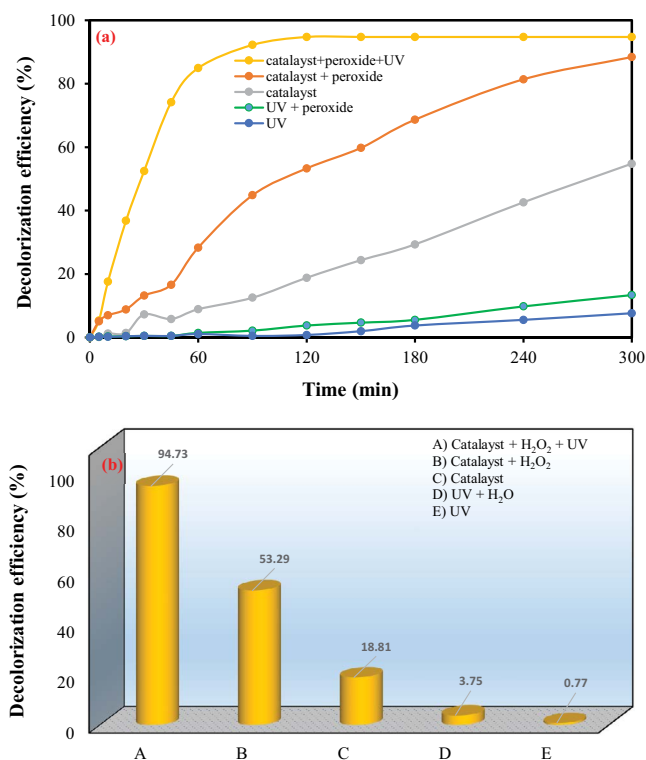


Fig. 15. Comparisons of various treatment processes for the degradation of MG during the photo-Fenton process (a) as a function of time and (b) for 120 min. Experimental conditions: natural hematite dosage: 0.50 g L⁻¹, [MG]₀ = 50 mg L⁻¹, temperature: 20°C, natural pH: 9.30 and [H₂O₂]₀ = 15 mM.

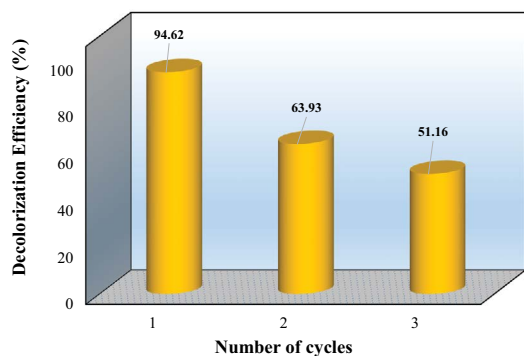


Fig. 16. Reusability of the catalyst within four consecutive experimental runs after 300 min. Experimental conditions: catalyst dosage = 3 g L⁻¹, [H₂O₂]₀ = 30 mM, [MG]₀ = 10 mg L⁻¹ and natural pH: 9.30.

As a result, the photo-Fenton process, which is the process of combining the light effect with the produced hydroxyl radicals, has shown a very good decolorization efficiency compared with other processes.

3.4.7. Reusability of the catalyst

From a practical point of view, the most important properties of catalyst is its long-term reusability. Therefore, reusability of the catalyst was also examined by three

consecutive cycles. The operational parameters were kept the same with the previous stage. After each cycle, the used catalyst was separated from the solution, washed with distilled water and dried for the next run. The decolorization efficiency of MG obtained for these three successive tests are demonstrated in Fig. 16. As seen from this figure, the efficiency reduced from 94.62% to 63.93% after three consecutive cycles, corresponding to only 51.16% decline in the efficiency. In addition, at the end of 18 h, the decolorization efficiency was found to have an approach of 98% at all three cycles. This result points out the reusability of the natural hematite particles as catalyst from aqueous solution.

4. Conclusion

In this study, natural hematite particles were used as heterogeneous catalyst in photo-Fenton process for the degradation of MG dye from aqueous solutions. XRD, FT-IR, SEM and EDX analyses confirmed the favorable structure of the prepared natural hematite as a catalyst. The experimental results conclude that:

- Natural hematite particles can effectively degrade MG dye by the photo-Fenton process.
- The photo-Fenton process provided the highest removal efficiency, 94.73%, among the various processes tested.
- The optimum values of catalyst dosage, peroxide concentration and initial dye concentration were sequentially found as 0.25 g L⁻¹, 15 mM and 10 mg L⁻¹.
- Excessive dosage of the catalyst reduced the decolorization efficiency of MG dye.
- High amount of peroxide usage caused a substantial decrease in the efficiency.
- The decolorization efficiency of MG at high pH was found to be much more effective than low pH. For example, when the pH of the solution decreased from 11 to 3, the decolorization effect of MG increased from 23.64% to 97.90%.

In conclusion, the natural hematite can be effectively used as heterogeneous catalyst in photo-Fenton process for the purification of water contaminated by MG dye.

Acknowledgments

The author would like to thank Ataturk University for Eastern Anatolian High Technology Application and Research Center (DAYTAM) from Ataturk University for technical analysis. In addition, I would like to thank my dear colleague, İlker ACAR, for his valuable support in English editing.

References

- [1] Z. Noorimotlagh, R. Darvishi Cheshmeh Soltani, A.R. Khataee, S. Shahriyar, H. Nourmoradi, Adsorption of a textile dye in aqueous phase using mesoporous activated carbon prepared from Iranian milk vetch, *J. Taiwan Inst. Chem. Eng.*, 45 (2014) 1783–1791.
- [2] A.A. Siyal, M.R. Shamsuddin, M.I. Khan, N.E. Rabat, M. Zulfiqar, Z. Man, J. Stame, K.A. Azizli, A review on geopolymers as emerging materials for the adsorption of heavy metals and dyes, *J. Environ. Manage.*, 224 (2018) 327–339.

- [3] R. Darvishi Cheshmeh Soltani, A.R. Khataee, M. Mashayekhi, Photocatalytic degradation of a textile dye in aqueous phase over ZnO nanoparticles embedded in biosilica nanobiostructure, *Desal. Wat. Treat.*, 57 (2016) 13494–13504.
- [4] S. Jorfi, G. Barzegar, M. Ahmadi, R. Darvishi Cheshmeh Soltani, N. alah Jafarzadeh Haghighifard, A. Takdastan, R. Saeedi, M. Abtahi, Enhanced coagulation-photocatalytic treatment of Acid red 73 dye and real textile wastewater using UVA/synthesized MgO nanoparticles, *J. Environ. Manage.*, 177 (2016) 111–118.
- [5] Y.L. Pang, S. Lim, H.C. Ong, W.T. Chong, Synthesis, characteristics and sonocatalytic activities of calcined γ -Fe₂O₃ and TiO₂ nanotubes/ γ -Fe₂O₃ magnetic catalysts in the degradation of Orange G, *Ultrason. Sonochem.*, 29 (2016) 317–327.
- [6] A. Khataee, A. Karimi, S. Arefi-Oskoui, R. Darvishi Cheshmeh Soltani, Y. Hanifehpour, B. Soltani, S.W. Joo, Sonochemical synthesis of Pr-doped ZnO nanoparticles for sonocatalytic degradation of Acid Red 17, *Ultrason. Sonochem.*, 22 (2015) 371–381.
- [7] H. Zhang, H. Fu, D. Zhang, Degradation of C.I. Acid Orange 7 by ultrasound enhanced heterogeneous Fenton-like process, *J. Hazard. Mater.*, 172 (2009) 654–660.
- [8] H. Hassan, B.H. Hameed, Fe-clay as effective heterogeneous Fenton catalyst for the decolorization of Reactive Blue 4, *Chem. Eng. J.*, 171 (2011) 912–918.
- [9] J.L. Wang, L.J. Xu, Advanced oxidation processes for wastewater treatment: formation of hydroxyl radical and application, *Crit. Rev. Env. Sci. Technol.*, 42 (2012) 251–325.
- [10] M. Klavarioti, D. Mantzavinos, D. Kassinos, Removal of residual pharmaceuticals from aqueous systems by advanced oxidation processes, *Environ. Int.*, 35 (2009) 402–417.
- [11] M. Petkovšek, M. Zupanc, M. Dular, T. Kosjek, E. Heath, B. Kompare, B. Širok, Rotation generator of hydrodynamic cavitation for water treatment, *Sep. Purif. Technol.*, 118 (2013) 415–423.
- [12] S. Malato, P. Fernández-Ibáñez, M.I. Maldonado, J. Blanco, W. Gernjak, Decontamination and disinfection of water by solar photocatalysis: recent overview and trends, *Catal. Today*, 147 (2009) 1–59.
- [13] N. Klamerth, S. Malato, A. Agüera, A. Fernández-Alba, Photo-Fenton and modified photo-Fenton at neutral pH for the treatment of emerging contaminants in wastewater treatment plant effluents: a comparison, *Water Res.*, 47 (2013) 833–840.
- [14] L. Prieto-Rodríguez, D. Spasiano, I. Oller, I. Fernández-Calderero, A. Agüera, S. Malato, Solar photo-Fenton optimization for the treatment of MWTP effluents containing emerging contaminants, *Catal. Today*, 209 (2013) 188–194.
- [15] C. von Sonntag, The basics of oxidants in water treatment. Part A: OH radical reactions, *Water Sci. Technol.*, 55 (2007) 19–23.
- [16] M.A. Rauf, S.S. Ashraf, Radiation induced degradation of dyes—an overview, *J. Hazard. Mater.*, 166 (2009) 6–16.
- [17] S.M. Kumar, Degradation and mineralization of organic contaminants by Fenton and photo-Fenton processes: review of mechanisms and effects of organic and inorganic additives, *Res. J. Chem. Environ.*, 15 (2011) 96–112.
- [18] J.I. Nieto-Juarez, T. Kohn, Virus removal and inactivation by iron (hydr) oxide-mediated Fenton-like processes under sunlight and in the dark, *Photochem. Photobiol. Sci.*, 12 (2013) 1596–1605.
- [19] L. Demarchis, M. Minella, R. Nisticò, V. Maurino, C. Minero, D. Vione, Photo-Fenton reaction in the presence of morphologically controlled hematite as iron source, *J. Photochem. Photobiol., A*, 307–308 (2015) 99–107.
- [20] H. Bataineh, O. Pestovsky, A. Bakac, pH-induced mechanistic changeover from hydroxyl radicals to iron(IV) in the Fenton reaction, *Chem. Sci.*, 3 (2012) 1594–1599.
- [21] J. Gomis, R.F. Vercher, A.M. Amat, D.O. Mártire, M.C. González, A. Bianco Prevot, E. Montoneri, A. Arques, L. Carlos, Application of soluble bio-organic substances (SBO) as photocatalysts for wastewater treatment: sensitizing effect and photo-Fenton-like process, *Catal. Today*, 209 (2013) 176–180.
- [22] C. Minero, M. Lucchiari, V. Maurino, D. Vione, A quantitative assessment of the production of •OH and additional oxidants in the dark Fenton reaction: Fenton degradation of aromatic amines, *RSC Adv.*, 3 (2013) 26443–26450.
- [23] A.M.T. Silva, J. Herney-Ramirez, U. Söylemez, L.M. Madeira, A lumped kinetic model based on the Fermi's equation applied to the catalytic wet hydrogen peroxide oxidation of Acid Orange 7, *Appl. Catal., B*, 121–122 (2012) 10–19.
- [24] M. Mishra, D.-M. Chun, α -Fe₂O₃ as a photocatalytic material: a review, *Appl. Catal., A*, 498 (2015) 126–141.
- [25] Y.Y. Liu, W. Jin, Y.P. Zhao, G.S. Zhang, W. Zhang, Enhanced catalytic degradation of methylene blue by α -Fe₂O₃/graphene oxide via heterogeneous photo-Fenton reactions, *Appl. Catal., B*, 206 (2017) 642–652.
- [26] A. Gajović, A.M.T. Silva, R.A. Segundo, S. Šturm, B. Jančar, M. Čeh, Tailoring the phase composition and morphology of Bi-doped goethite-hematite nanostructures and their catalytic activity in the degradation of an actual pesticide using a photo-Fenton-like process, *Appl. Catal., B*, 103 (2011) 351–361.
- [27] Y. Bessekhouad, D. Robert, J.V. Weber, N. Chaoui, Effect of alkaline-doped TiO₂ on photocatalytic efficiency, *J. Photochem. Photobiol., A*, 167 (2004) 49–57.
- [28] S. Zeng, K. Tang, T. Li, Z. Liang, D. Wang, Y. Wang, W. Zhou, Hematite hollow spindles and microspheres: Selective synthesis, growth mechanisms, and application in lithium ion battery and water treatment, *J. Phys. Chem. C*, 111 (2007) 10217–10225.
- [29] M. Zainuri, Hematite from Natural Iron Stones as Microwave Absorbing Material on X-Band Frequency Ranges, *IOP Conference Series: Materials Science and Engineering*, IOP Publishing, 2017.
- [30] N.M. Khalil, E.E. Saad, A.I. Alasfar, H.A. Saleh, Chemical and mineralogical study of south-Libyan hematite ore, *Int. J. Eng. Innovation Technol.*, 2 (2012) 36–38.
- [31] E.M. El Afifi, M.F. Attallah, E.H. Borai, Utilization of natural hematite as reactive barrier for immobilization of radionuclides from radioactive liquid waste, *J. Environ. Radioact.*, 151 (2016) 156–165.
- [32] B. Lu, Surface Reactivity of Hematite Nanoparticles, *M.Sc. Thesis* 45 ECTS, S901 87 Umea, Sweden, 2014.
- [33] A. Hassani, M. Karaca, S. Karaca, A. Khataee, O. Acisli, B. Yilmaz, Preparation of magnetite nanoparticles by high-energy planetary ball mill and its application for ciprofloxacin degradation through heterogeneous Fenton process, *J. Environ. Manage.*, 211 (2018) 53–62.
- [34] A. Hassani, C. Karaca, S. Karaca, A. Khataee, O. Acisli, B. Yilmaz, Enhanced removal of basic violet 10 by heterogeneous sono-Fenton process using magnetite nanoparticles, *Ultrason. Sonochem.*, 42 (2018) 390–402.
- [35] M. Thommes, K. Kaneko, A.V. Neimark, J.P. Olivier, F. Rodriguez-Reinoso, J. Rouquerol, K.S. Sing, Physisorption of gases, with special reference to the evaluation of surface area and pore size distribution (IUPAC Technical Report), *Pure Appl. Chem.*, 87 (2015) 1051–1069.
- [36] O. Acisli, A. Khataee, R. Darvishi Cheshmeh Soltani, S. Karaca, Ultrasound-assisted Fenton process using siderite nanoparticles prepared via planetary ball milling for removal of reactive yellow 81 in aqueous phase, *Ultrason. Sonochem.*, 35 (2017) 210–218.
- [37] S. Fathinia, M. Fathinia, A.A. Rahmani, A. Khataee, Preparation of natural pyrite nanoparticles by high energy planetary ball milling as a nanocatalyst for heterogeneous Fenton process, *Appl. Surf. Sci.*, 327 (2015) 190–200.
- [38] M.N. Chong, B. Jin, C.W. Chow, C. Saint, Recent developments in photocatalytic water treatment technology: a review, *Water Res.*, 44 (2010) 2997–3027.
- [39] M. Umar, H.A. Aziz, Photocatalytic Degradation of Organic Pollutants in Water, in *Organic Pollutants - Monitoring, Risk and Treatment*, IntechOpen, 2013, pp. 195–208.
- [40] H. Mechakra, T. Sehilli, M.A. Kribeche, A.A. Ayachi, S. Rossignol, C. George, Use of natural iron oxide as heterogeneous catalyst in photo-Fenton-like oxidation of chlorophenylurea herbicide in aqueous solution: reaction monitoring and degradation pathways, *J. Photochem. Photobiol., A*, 317 (2016) 140–150.

- [41] D. Bahnemann, Photocatalytic water treatment: solar energy applications, *Solar Energy*, 77 (2004) 445–459.
- [42] M. Saquib, M. Muneer, TiO₂-mediated photocatalytic degradation of a triphenylmethane dye (gentian violet), in aqueous suspensions, *Dyes Pigm.*, 56 (2003) 37–49.
- [43] U.I. Gaya, A.H. Abdullah, Heterogeneous photocatalytic degradation of organic contaminants over titanium dioxide: a review of fundamentals, progress and problems, *J. Photochem. Photobiol., C*, 9 (2008) 1–12.
- [44] M. Karaca, M. Kıranşan, S. Karaca, A. Khataee, A. Karimi, Sonocatalytic removal of naproxen by synthesized zinc oxide nanoparticles on montmorillonite, *Ultrason. Sonochem.*, 31 (2016) 250–256.
- [45] R. Darvishi Cheshmeh Soltani, M. Safari, M. Mashayekhi, Sonocatalyzed decolorization of synthetic textile wastewater using sonochemically synthesized MgO nanostructures, *Ultrason. Sonochem.*, 30 (2016) 123–131.
- [46] O. Acisli, A. Khataee, S. Karaca, M. Sheydaei, Modification of nanosized natural montmorillonite for ultrasound-enhanced adsorption of Acid Red 17, *Ultrason. Sonochem.*, 31 (2016) 116–21.
- [47] H. Zhang, J. Zhang, C. Zhang, F. Liu, D. Zhang, Degradation of CI Acid Orange 7 by the advanced Fenton process in combination with ultrasonic irradiation, *Ultrason. Sonochem.*, 16 (2009) 325–330.
- [48] A. Öztürk, E. Malkoc, Adsorptive potential of cationic Basic Yellow 2 (BY2) dye onto natural untreated clay (NUC) from aqueous phase: mass transfer analysis, kinetic and equilibrium profile, *Appl. Surf. Sci.*, 299 (2014) 105–115.
- [49] L. Leng, X. Yuan, G. Zeng, J. Shao, X. Chen, Z. Wu, H. Wang, X. Peng, Surface characterization of rice husk bio-char produced by liquefaction and application for cationic dye (Malachite green) adsorption, *Fuel*, 155 (2015) 77–85.
- [50] L. Hou, L. Wang, S. Royer, H. Zhang, Ultrasound-assisted heterogeneous Fenton-like degradation of tetracycline over a magnetite catalyst, *J. Hazard. Mater.*, 302 (2016) 458–467.
- [51] R. Molina, F. Martínez, J.A. Melero, D.H. Bremner, A.G. Chakinala, Mineralization of phenol by a heterogeneous ultrasound/Fe-SBA-15/H₂O₂ process: multivariate study by factorial design of experiments, *Appl. Catal., B*, 66 (2006) 198–207.
- [52] Y.P. Zhang, K.T. Dong, Z. Liu, H.L. Wang, S.X. Ma, A.Y. Zhang, M. Li, L.Q. Yu, Y. Li, Sulfurized hematite for photo-Fenton catalysis, *Prog. Nat. Sci. - Mater. Int.*, 27 (2017) 443–451.
- [53] H. Xie, Y. Li, S. Jin, J. Han, X. Zhao, Facile fabrication of 3D-ordered macroporous nanocrystalline iron oxide films with highly efficient visible light induced photocatalytic activity, *J. Phys. Chem. C*, 114 (2010) 9706–9712.
- [54] J. Yu, X. Yu, B. Huang, X. Zhang, Y. Dai, Hydrothermal synthesis and visible-light photocatalytic activity of novel cage-like ferric oxide hollow spheres, *Cryst. Growth Des.*, 9 (2009) 1474–1480.
- [55] X. Zhou, H. Yang, C. Wang, X. Mao, Y. Wang, Y. Yang, G. Liu, Visible light induced photocatalytic degradation of rhodamine B on one-dimensional iron oxide particles, *J. Phys. Chem. C*, 114 (2010) 17051–17061.
- [56] X. Zhou, J. Lan, G. Liu, K. Deng, Y. Yang, G. Nie, J. Yu, L. Zhi, Facet-mediated photodegradation of organic dye over hematite architectures by visible light, *Angew. Chem.*, 124 (2012) 182–186.